PCCP

# 31P Spin-Lattice and Singlet Order Relaxation Mechanisms in Pyrophosphate Studied by Isotopic Substitution, Field Shuttling NMR, and Molecular Dynamics Simulation



| | |
|---|---|
| Journal: | *Physical Chemistry Chemical Physics* |
| Manuscript ID | CP-ART-08-2022-003801.R1 |
| Article Type: | Paper |
| Date Submitted by the Author: | 13-Sep-2022 |
| Complete List of Authors: | Korenchan, David; New York University, Chemistry<br>Lu, Jiaqi; New York University, Chemistry<br>Sabba, Mohamed; University of Southampton, School of Chemistry<br>Dagys, Laurynas; University of Southampton,<br>Brown, Lynda; University of Southampton, School of Chemistry<br>Levitt, Malcolm; University of Southampton, School of Chemistry<br>Jerschow, Alexej; New York University, Chemistry |
| | |

ARTICLE

# $^{31}$P Spin-Lattice and Singlet Order Relaxation Mechanisms in Pyrophosphate Studied by Isotopic Substitution, Field Shuttling NMR, and Molecular Dynamics Simulation

Received 00th January 20xx,
Accepted 00th January 20xx

DOI: 10.1039/x0xx00000x

David E. Korenchan,†[a] Jiaqi Lu,†[a] Mohamed Sabba,[b] Laurynas Dagys,[b] Lynda J. Brown,[b] Malcolm H. Levitt,[b] and Alexej Jerschow*[a]

Nuclear spin relaxation mechanisms are often difficult to isolate and identify, especially in molecules with internal flexibility. Here we combine experimental work with computation in order to determine the major mechanisms responsible for $^{31}$P spin-lattice and singlet order (SO) relaxation in pyrophosphate, a physiologically relevant molecule. Using field-shuttling relaxation measurements (from 2 $\mu$T to 9.4 T) and rates calculated from molecular dynamics (MD) trajectories, we identified chemical shift anisotropy (CSA) and spin-rotation as the major mechanisms, with minor contributions from intra- and intermolecular coupling. The significant spin-rotation interaction is a consequence of the relatively rapid rotation of the -$PO_3^{2-}$ entities around the bridging P-O bonds, and is treated by a combination of MD simulations and quantum chemistry calculations. Spin-lattice relaxation was predicted well without adjustable parameters, and for SO relaxation one parameter was extracted from the comparison between experiment and computation (a correlation coefficient between the rotational groups).

## Introduction

Nuclear spin relaxation holds a wealth of information about the dynamics of chemical systems. The main contributions to relaxation include chemical shift anisotropy (CSA), dipolar coupling interactions, paramagnetic interactions, and, for highly mobile molecules (especially in the gas phase), spin-rotation interactions.[2] Disentangling the relative contributions of each can be difficult, and the spin-rotation mechanism has been under-explored, especially in flexible molecules in solution.[3, 4] Progress has been made recently in accurately computing relaxation rates with molecular dynamics (MD) simulations and *ab initio* calculations in small molecules and ions,[5-9] and it has been demonstrated that very few (if any) adjustable parameters may be required in order to do so.[9]

Nuclear spin singlet order (SO) relaxation has been of particular interest, since it offers the opportunity of potentially achieving particularly long magnetization storage mechanisms (the SO relaxation time $T_S$ has been shown in some cases to be up to two orders of magnitude larger than $T_1$).[10-18] As a result, SO relaxation can be diagnostic of particularly weak relaxation mechanisms.[9] The underlying reason is that the spin symmetry of such states can eliminate the strongest relaxation mechanisms.[19-22] The study of nuclear singlet order has led to new applications in hyperpolarization,[23, 24] contrast development for imaging,[25] measurement of slow processes such as molecular rearrangement,[26] diffusion,[27] and bond rotation,[28] the development of new pulse sequences,[26, 29-36] and spectral editing.[33, 37, 38]

Very recently, $^{31}$P spin-lattice and SO relaxation have been studied in large diphosphate compounds.[8, 39] For the $^{31}$P spins in the compounds studied, however, SO relaxation has been found to be more rapid than spin-lattice relaxation, with a major reason being the anticorrelation between the chemical shift anisotropy (CSA) tensors of the two spins.[8]

Two aspects of this prior work motivated us to examine $^{31}$P-spin relaxation further. The compounds used previously were particularly bulky and contained large asymmetries between the two spins (either transient or constant). We therefore sought to study the small, highly symmetric molecule pyrophosphate, modified to have slight asymmetry, thereby enabling access to SO. The molecule was further considered due to its physiological relevance. An additional aspect motivating this study was the proposal that $^{31}$P nuclear spin states could be of relevance in physiological processes, hypothesized to include cognition.[40]

Since the main mechanism in prior work on substituted phosphates appeared to be due to CSA, we wished to perform magnetic field-dependent studies. We present here Zeeman and SO relaxation studies over a large field range (2 $\mu$T to 9.4 T) to investigate the major relaxation mechanisms as a function of magnetic field and determine the low-field limit to these relaxation rates. We further identify the mechanistic contributions to these relaxation rates by MD simulations and *ab initio* computation, and we demonstrate that both the CSA

[a] *Department of Chemistry, New York University, 100 Washington Square E, New York, NY 10003.*
[b] *School of Chemistry, University of Southampton, Southampton SO17 1BJ, UK.*
† These authors contributed equally.
Electronic Supplementary Information [1] available: [details of any supplementary information available should be included here]. See DOI: 10.1039/x0xx00000x

and spin-rotation contributions can be derived successfully from the simulations with only one adjustable parameter.

## Results

### Preparation and characterization of slightly chemically inequivalent pyrophosphate

One challenge in the study of SO in the pyrophosphate ($PP_i$) molecule is the lack of inequivalence (either chemical or magnetic), which is needed for creating and reading out SO of the $^{31}P$ spins. To overcome this challenge, we unsymmetrically labeled $PP_i$ with the $^{18}O$ isotope. The increased mass of the $^{18}O$ nuclei relative to the abundant $^{16}O$ isotope was expected to induce a small chemical shift difference between the neighboring $^{31}P$ nuclei, sufficiently large to allow creation and read-out of SO. This strategy was used previously for pairs of $^{13}C$ nuclei.[41] The tetrasodium salt of the unsymmetrically labelled $^{18}O$-$PP_i$ ($uPP_i$) was synthesized and prepared in $D_2O$ under highly alkaline conditions (for details, see Materials and Methods section) to avoid potentially interfering effects due to proton exchange, which can accelerate SO relaxation.[42] The addition of 10 equivalents of potassium hydroxide (KOH) was found to promote longer SO lifetimes between the $uPP_i$ $^{31}P$ nuclei (Fig. S1, ESI). Similar results were obtained by adding ethylenediaminetetraacetate (EDTA) instead (Fig. S1, ESI).

The NMR properties of the synthesized $uPP_i$ $^{31}P$ spin system were extracted from a $^{31}P$ pulse-acquire spectrum acquired at 9.4 T by multiplet simulation and fitting using the Spinach MATLAB package (http://spindynamics.org/group/).[43] Fig. 1 displays the fitting results. The unsymmetrical isotopic labelling of the $uPP_i$ induces a slight chemical shift difference $\Delta\delta_{PP}$ between the two $^{31}P$ nuclei of 0.0663 ppm, or 10.7 Hz at 9.4 T. The $^{31}P$ nuclei share a homonuclear *J*-coupling of magnitude $^2J_{PP}$ = 21.5 Hz. Thus, the $uPP_i$ $^{31}P$ spin system is in a strongly coupled regime at 9.4 T. Singlet-triplet mixing can occur at high fields, but this mechanism of SO decay is eliminated when the sample is moved to lower fields. Additional peaks are observed which likely stem from partial labelling of the molecule. We could not fully identify these, but products with partial labelling should not affect the results, since the triplet-singlet transfer is tailored to a particular chemical shift / coupling combination. The isotope composition should not affect relaxation rates due to the small differences in mass. The $^{31}P$ $R_1$ values of the unlabeled $PP_i$ and the $^{18}O$-labeled $uPP_i$ measured at 9.4 T were 0.107 $s^{-1}$ and 0.102 $s^{-1}$, respectively, with identical solution conditions (pD 14.4, 25 °C).

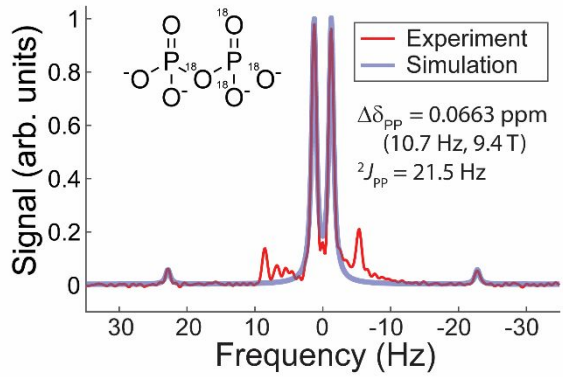


**Fig. 1** $^{31}P$ NMR spectrum and fitting results of fully deprotonated unsymmetrical pyrophosphate in KOH and $D_2O$. Additional unidentified peaks arising from the synthesis besides the inner and outer doublet of doublet peaks were excluded from fitting. Fitted $^{31}P$ chemical shift difference and homonuclear *J*-coupling values are displayed to the right of the spectra. The structure of the unsymmetric pyrophosphate is shown on the top left.

### NMR field-cycling relaxation measurements of $uPP_i$

We then performed $^{31}P$ field-dependent relaxation measurements of both spin-lattice and SO relaxation, in order to compare and contrast known relaxation mechanisms. The spin lattice relaxation rate constant $R_1$ (= $1/T_1$) was measured using an inversion-recovery pulse sequence. For the measurement of the SO relaxation rate $R_S$ (= $1/T_S$), we chose to utilize the spin-lock induced crossing (SLIC) pulse sequence[32] for preparing and reading out SO for NMR spectroscopic relaxation measurements. Instrumentation details are described in the Materials and Methods section. The SLIC pulse sequence used for field-dependent measurements of $R_S$ is displayed in Fig. 2. Optimization of the SLIC spin-lock pulse power and duration confirmed the spin system parameters determined via spectral fitting: the optimal pulse amplitude and duration corresponded with $^2J_{PP}$ of 20.3 Hz and a $\Delta\delta_{PP}$ of 12.3 Hz (Fig. S2, ESI).

The results of the relaxation measurements are shown in Fig. 3. Generally, the $R_1$ and $R_S$ values tracked each other, with $R_1$ experiencing a slight increase in the 2 μT to 200 mT range. $R_S$ also tended to be smaller than $R_1$ in the high-field regime, above 4.5 T. Both $R_1$ and $R_S$ approached a constant relaxation rate offset of approximately 0.018 $s^{-1}$ at the lowest field values measured. The measured relaxation trends with magnetic field were well approximated using MD simulations and *ab initio* calculation (Fig. 3, dashed lines), as described below.

### Molecular dynamics simulation and *ab initio* calculation of relaxation rate curves

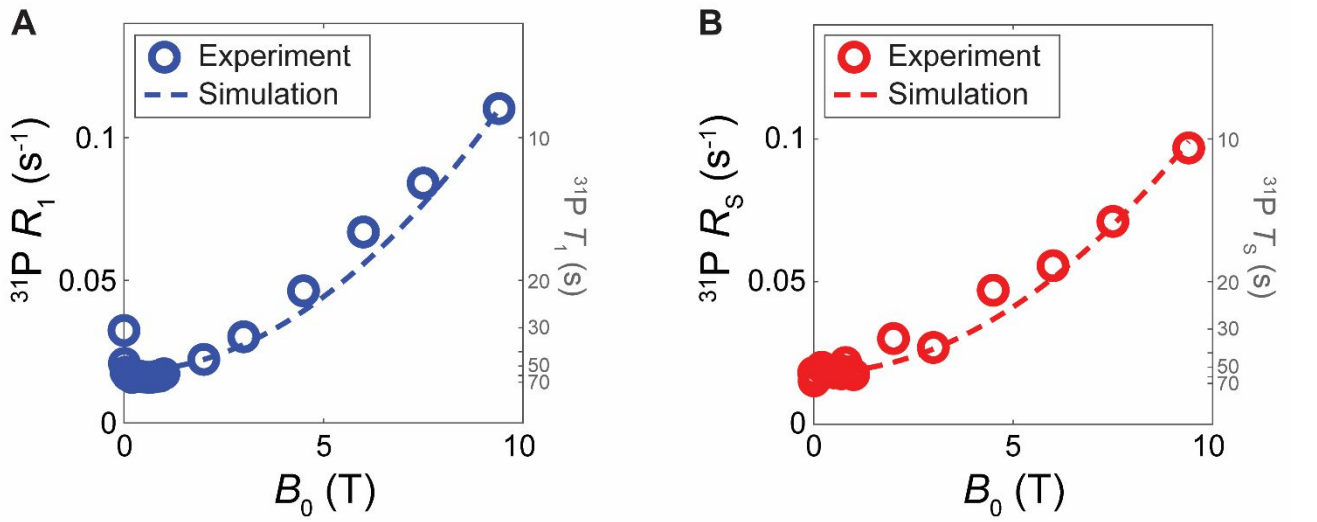


**Fig. 3** $^{31}$P NMR relaxation measurements of fully deprotonated 30 mM unsymmetrical pyrophosphate as a function of magnetic field strength. (A) spin-lattice relaxation; (B) SO relaxation. Open circles indicate experimental measurements, and dashed lines indicate the total simulated relaxation curve. For each plot, time constant values are shown on the right y-axis which correspond with the relaxation rate values on the left y-axis.

In order to study the CSA tensors in uPP$_i$ and their contributions to longitudinal and SO relaxation, MD simulations were performed using Gaussian 16 and Amber20[44] software, as described in the Materials and Methods section. Fig. 4 shows average and multiple-snapshot representations of the symmetric portion of the CSA tensors experienced by the $^{31}$P nuclei. The CSA tensor visualizations show that the principal component appears almost completely aligned with the bond between phosphorus and the bridging oxygen. Because the -$PO_3^{2-}$ groups experience fast intramolecular rotation about the bridging P-O bond (see Fig. 4B), the CSA tensors were averaged across the 100 conformations, following molecular alignment along the P-P vector. A more detailed justification for this averaging procedure can be found in the Materials and Methods section. The difference between the average tensors at each $^{31}$P nucleus was computed, and the average and difference tensors were separated into their symmetric and antisymmetric components. The (Frobenius) norms of the tensor components are summarized in Table 1 and were used to calculate the CSA contributions to $R_1$ and $R_S$ using the expressions

**Table 1** Frobenius norms of uPP$_i$ chemical shift anisotropy tensor averages from *ab initio* calculation on snapshots from MD simulations.

| CSA tensor component | Norm of individual tensor averages (ppm) | Norm of difference tensor averages (ppm) |
|---|---|---|
| Symmetric | 92.8 | 79.6 |
| Antisymmetric | 9.1 | 18.2 |

$$R_1^{sym} = \frac{2}{15}\left(\omega_0\sqrt{\frac{3}{2}}\|\sigma_{sym}\|_F\right)^2 \frac{\tau_2}{1+(\omega_0\tau_2)^2} \quad (1)$$

$$R_1^{anti} = \frac{1}{6}(\omega_0\|\sigma_{anti}\|_F)^2 \frac{\tau_1}{1+(3\omega_0\tau_1)^2} \quad (2)$$

$$R_S^{sym} = \frac{2}{9}(\omega_0\|\Delta\sigma_{sym}\|_F)^2 \frac{1}{5}\left(2\tau_2 + \frac{3\tau_2}{1+(\omega_0\tau_2)^2}\right) \quad (3)$$

$$R_S^{anti} = \frac{2}{9}(\omega_0\|\Delta\sigma_{anti}\|_F)^2 \frac{\tau_1}{1+(3\omega_0\tau_1)^2}. \quad (4)$$

These expressions have been first given in Ref.[45] for the fast motion regime, and have later been provided outside of the fast motion regime in Ref.[46] in this form. In the equations above, $\omega_0$ is the Larmor frequency, $\|\sigma\|_F$ and $\|\Delta\sigma\|_F$ indicate the Frobenius norms of the average and difference tensors, respectively, and $\tau_1$ and $\tau_2$ are the first- and second-rank correlation times, respectively, where $\tau_1 = 3\tau_2$ assuming isotropic rotational diffusion.[1] The second-rank correlation time was determined to be 48.6 ps, based upon MD simulation following adjustment using the NMR-measured PP$_i$ diffusion coefficient, as described in the Materials and Methods section.

It is seen that CSA accounts for the major relaxation effect at high magnetic fields. The symmetric CSA component (Fig. 5, solid lines) contributes the most to $R_1$ and $R_S$ at high field strengths, whereas the antisymmetric contribution (Fig. 5, dotted lines) is relatively small for both but much larger for $R_S$ than it is for $R_1$. Other smaller, yet significant relaxation contributions, largely field-independent, are described further below.

The spin-rotation contribution to $R_1$ was calculated as follows: From MD simulations, the correlation function $\overline{\omega(0)\omega(t)}$ for the angular rotation frequency of the -$PO_3^{2-}$ entity about the bridging P-O bond of PP$_i$ was calculated. An exponential fit was performed to this function, which yielded $\overline{\omega(0)^2}$ and the correlation time $\tau_J$. These values were determined as 3.1 rad$^2$ps$^{-2}$ and 0.0255 ps, respectively. Gaussian 16 was used to compute the spin-rotation tensor for $^{31}$P in PP$_i$ at the B3LYP/aug-cc-pVTZ level, which produced the value for $C_\parallel/2\pi$ = 4.424 kHz, for rotation around the bridging P-O vector, and roughly two equivalent values for the perpendicular rotation $C_\perp/2\pi$ = 1.095 kHz. The spin-rotation tensors are visualized in Fig. S3 in the ESI, which indicates that the major component of this tensor also points along the bridging P-O bond similar to the CSA tensor. Given that the

motion perpendicular to the P-O bond can be assumed to be very small by comparison (see Fig. 4B, showing the superposition of conformers obtained from MD trajectories), we neglect this portion and calculate the spin-rotation relaxation rate constant by the expression

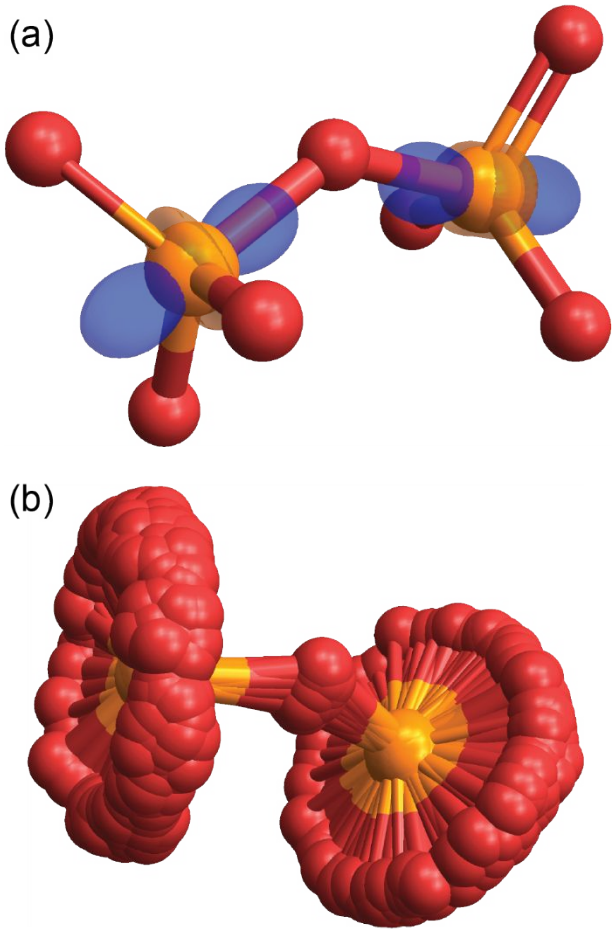


**Fig. 4** Graphical representations of $uPP_i$ molecular dynamics. (**A**) Ovaloid representation of the symmetric CSA tensor components experienced by each $^{31}P$ nucleus. (**B**) Combined snapshots of conformations sampled by the $uPP_i$ molecule within the molecular dynamics simulation, aligned along the P-P vector.

$$R_1^{SR} = \frac{2}{3\hbar^2}\overline{\omega(0)^2} I_{\parallel}^2 C_{\parallel}^2 \tau_J, \qquad (5)$$

where $I_{||}$ = 1.758·10$^{-45}$ kg m$^2$ is the moment of inertia for the -$PO_3^{2-}$ entity with respect to the bridging P-O axis. A derivation based on Pileio[47] and a consistency check with McClung[48] and Spiess[49] are provided in the ESI. The spin-rotation relaxation rate constant then becomes $R_1^{SR}$ = 0.0113 s$^{-1}$. The rate is essentially independent of the magnetic field due to the extremely short correlation time for the angular frequency correlation function.

Spin-rotation is also expected to affect the relaxation of SO in $uPP_i$. We made the following considerations: were the spin-rotation field fluctuations produced by each rotating -$PO_3^{2-}$ group fully uncorrelated, we would predict $R_S^{SR}$ to be twice as large as $R_1^{SR}$. However, in this case $R_S$ would be larger than $R_1$ at low field strengths, whereas experimentally we observed similar low-field values of $R_1$ and $R_S$. We therefore determined the correlation coefficient $\alpha$ for the spin-rotation interaction at each $^{31}P$ spin following the discussion about correlated mechanisms of Tayler et al,[50] in particular Eqs. (1) and (2). From these considerations, one can obtain $R_S^{SR}/R_1^{SR} = 2(1-\alpha)$, as described in the derivation in the ESI. When using the experimental values for $R_S^{SR}$ and $R_1^{SR}$ we obtain the correlation coefficient $\alpha$ = 0.5. Modelling the spin-rotation contribution to $R_S$ in this manner produced an excellent fit to the experimental data (Fig. 3, dashed line). Other known relaxation contributions to $R_1$ and $R_S$ are described below.

MD simulations following the procedure of Kharkov et al[9] gave the contribution of intermolecular dipolar relaxation between $^{31}P$ and $^{2}D$ solvent spins as 5.14·10$^{-3}$ s$^{-1}$. The $^{31}P$-$^{31}P$ dipolar relaxation contribution, relevant only for $R_1$, was determined to be 1.60·10$^{-3}$ s$^{-1}$. The correlation times for these processes range from 20-40 ps, and therefore their contributions are likewise almost completely independent of the magnetic field. The singlet-triplet leakage (STL) contribution to SO relaxation cannot easily be determined in closed form, since it depends on the specifics of the other relaxation mechanisms. This effect was therefore estimated using the Spinach NMR simulation package in MATLAB[43], by simulating SO relaxation with and without the chemical shift difference included and calculating the difference. The contribution is field-dependent but relatively minor, as seen in Fig. 5. Finally, the $^{1}H$-$^{31}P$ dipolar relaxation contribution arising from the added KOH was estimated from the $^{2}D$-$^{31}P$ contribution as 0.00025 s$^{-1}$, which is negligible compared to other relaxation contributions.

## Discussion

Our $R_1$ and $R_S$ measurements show that $uPP_i$ high-field relaxation is dominated by the CSA mechanism, similar to the case in other reported diphosphates.[8, 39] In contrast to previous studies, however, the $R_S$ values observed in the high field regime are slightly lower compared with $R_1$. This finding corresponds well with the symmetric CSA tensor norm being somewhat lower for the difference tensor (Table 1). The norm of the antisymmetric component, however, is significantly larger for the difference tensors than for the individual tensors, with the result being a larger antisymmetric CSA contribution to $R_S$. Still, the antisymmetric contribution to $R_S$ is smaller than one fifth of the symmetric contribution.

Importantly, we observed that towards low fields, a constant offset in the relaxation rate constants is approached for the experimentally measured values of both $R_1$ and $R_S$. The offset at the lowest field, 2 $\mu$T, was found to be approximately 0.018 s$^{-1}$ for both. The same trend and similar, albeit slightly higher $R_1$ and $R_S$ offsets were observed from measurements on a 30 mM $uPP_i$ sample with 10 mM EDTA added (Fig. S4, ESI). We believe this constant contribution at the lowest field to be primarily comprised of spin-rotation relaxation, as shown in Fig. 5. Furthermore, at very low field strengths (2 μT to 100 mT), $R_1$ showed a peculiar increase in the rate that was consistently observed across different sample formulations (Fig. S4A). This effect is not understood at this time.

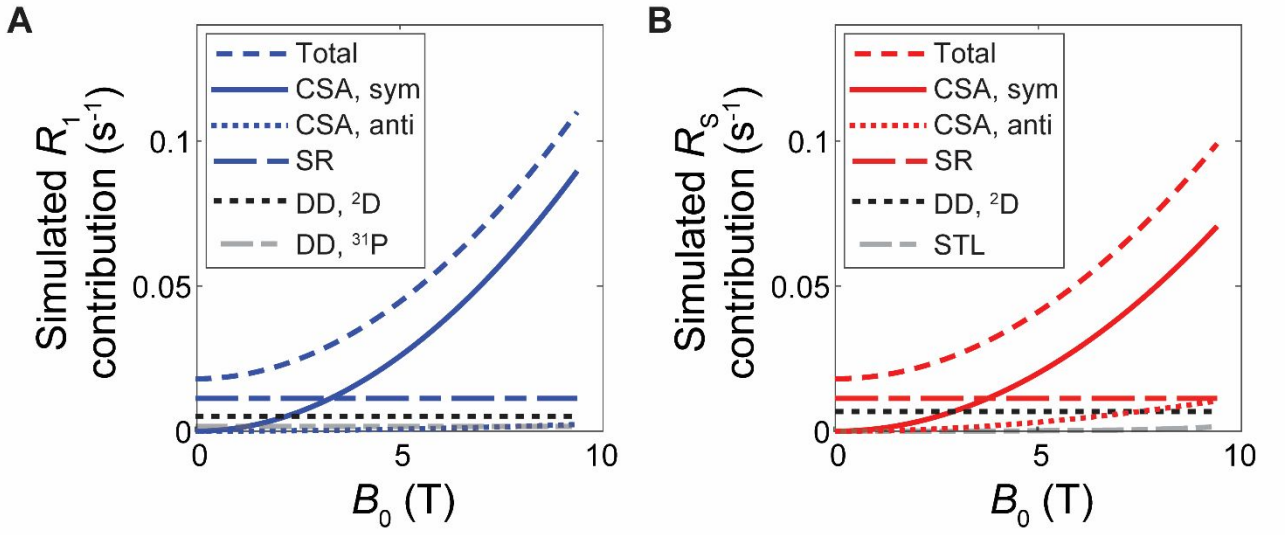


**Fig. 5** Breakdown of total simulated relaxation curve into components by relaxation mechanism. (**A**) calculated spin-lattice relaxation contributions; (**B**) calculated SO relaxation contributions. CSA = chemical shift anisotropy; SR = spin-rotation; DD = dipole-dipole relaxation; STL = singlet-triplet leakage.

Although our study was motivated by the biological relevance of pyrophosphate, we note that many of the experimental conditions used for our relaxation measurements are different from those that would be encountered in a biological system. First, our experiments were performed at a relatively high pD, to limit deuteron exchange. At physiological pH values one can observe reduced $T_S$ and $T_1$ relaxation times (similar to the case studied previously[42]). In addition, the nature of the counterion might play a minor role in the relaxation measurements. Slightly longer $T_1$ times were observed when KOH was used in the $uPP_i$ preparation, rather than NaOH (see ESI). Furthermore, $D_2O$ was used as a solvent rather than $H_2O$. We note that if $H_2O$ were used as a solvent, the lifetime limit would be significantly smaller. We measured an increase in $R_1$ of 0.028 $s^{-1}$ at 9.4 T when we replaced $D_2O$ with 90% $H_2O$ plus 10% $D_2O$. Assuming this increase to be field-independent, we would therefore expect a $T_1$ and $T_S$ maximum of approximately 26 s for this solvent. Finally, certain paramagnetic species are abundant within cells and tissues and can contribute to relaxation. Comparison of rates observed in degassed and non-degassed samples, however, showed approximately the same rate constants in the low field region, suggesting that the effect of paramagnetic relaxation due to oxygen is low (Fig. S4, ESI). Other paramagnetic impurities were considered, but careful and extensive cleaning of glassware with KOH/iPrOH and HCl did not produce significant changes. Examination of relaxation in the presence of EDTA (to potentially capture paramagnetic impurities) likewise did not show significant changes in the observed rate constants (Fig. S4, ESI).

## Conclusions

In summary, we report measurements of $^{31}$P Zeeman magnetization and SO decay in isotope labeling-induced unsymmetric $PP_i$ over a wide range of field strengths, with the largest values of the $T_1$ and $T_S$ time constants being approximately 65 s in the low field range. We demonstrate that CSA dominates both $R_1$ and $R_S$ relaxation at high fields and diminishes at low fields, and that the two rates have similar values from 2 μT to 9.4 T. We observe that both $R_1$ and $R_S$ approach a constant value at low field strengths, which appears to be primarily explained by spin-rotation relaxation, with minor (but non-negligible) contributions from intermolecular $^{31}$P-$^2$D dipolar coupling and intramolecular $^{31}$P-$^{31}$P dipolar coupling. The magnitude of the spin-rotation relaxation contribution in this molecular system was an unexpected discovery, related to the relatively rapid rotation of the $-PO_3^{2-}$ entities. In low magnetic fields the $^{31}$P singlet lifetime of pyrophosphate would possibly be long enough to sustain the entanglement of spin pairs in solution, and perhaps even mechanisms relevant for in quantum cognition.[40, 51] However, as far as the authors know, there is no evidence that cognition is significantly disturbed by high magnetic fields, as would be anticipated from the experimental results described here. Overall, these studies point to the importance of internal motions for the spin-rotation relaxation mechanism in flexible molecules in solution for both spin-lattice, and SO relaxation, and also to the possibility of accurately predicting relaxation rates from MD simulations.

## Materials and methods

### Unsymmetrically $^{18}$O-labeled pyrophosphate synthesis and formulation

The synthesis of $^{18}O/^{16}O$ unsymmetrical pyrophosphate tetrasodium salt **6**, henceforth referred to as $uPP_i$, is shown in Fig. S5. Light sensitive silver phosphate salt **1** was prepared from $^{18}$O phosphoric acid by a simple precipitation method.[52] Subsequent benzylation in the presence of excess benzyl chloride provided the triester **2** in 75% yield.[53] Heating triester **2** in the presence of one equivalent of sodium iodide in acetone accomplished selective mono-deprotection,[53] and the resulting dibenzyl phosphate sodium salt **3** was converted to the tetrabenzyl $^{18}O/^{16}O$ pyrophosphate **4** by reaction with dibenzyl

phosphoryl chloride ($^{16}O$, obtained by the chlorination of dibenzyl phosphite with NCS in benzene and used directly)[54] in the presence of triethylamine.[55] Global debenzylation of the tetrabenzyl pyrophosphate using hydrogen over Pd required prolonged reaction times and was inefficient due to accompanying partial hydrolysis to the orthophosphate. Ultimately, a two-step procedure via the dibenzyl pyrophosphate disodium salt **5** was optimised, with the remaining two benzyl groups removed by hydrogenolysis over Pd in the presence of sodium bicarbonate in 5 hours. This six-step sequence afforded the regioselectively $O^{18}/O^{16}$ labelled pyrophosphate tetrasodium salt **6** as a white crystalline solid. Isotopic incorporation was confirmed by mass spectrometry to be 96% $^{18}O_4$, 96% $^{18}O_3$.

For NMR experiments, the tetrabasic sodium $uPP_i$ was formulated as a 30 mM solution in deuterium oxide plus 10 equivalents of potassium hydroxide. The final concentrations of $Na^+$ and $K^+$ counterions were 120 mM and 300 mM, respectively. The pD of the solution was expected to be about 14.4, based upon room-temperature pH electrode measurements of a sample prepared identically but with unlabelled tetrabasic sodium pyrophosphate. The NMR tubes used with the samples were carefully cleaned to avoid any paramagnetic impurities by immersing in a KOH/iPrOH bath overnight followed by HCl immersion overnight, rinsing several times with acetone, and drying with argon gas. More details on sample preparation can be found in the ESI.

**Field-dependent NMR spectroscopy**

All field-dependent NMR measurements were performed at the University of Southampton, based on the design by Zhukov et al.[56] Approximately 300 μL of the $uPP_i$ solution were placed in a 5 mm NMR tube and measured using a 9.4 T Bruker NMR spectrometer equipped with a home-built shuttling system, used to transport the sample rapidly between regions of different magnetic field. The shuttling system included a shielded region above the magnet and therefore enabled access to magnetic field strengths as low as 2 μT. Spin-lattice relaxation was measured using an inversion-recovery sequence with magnetic field shuttling during the waiting time. SO was prepared with a spin-lock induced crossing (SLIC) spin-lock pulse[32] at 9.4 T within the bore, the sample was shuttled to a region above the magnet for SO relaxation at the desired field strength, and then returned to the magnet bore for SO readout via SLIC (Fig. 1). The sample shuttling speed to and from the low field for all measurements was about 1 m/s, and the shuttling time (one-way) was no greater than 1 second. The sensitivity of singlet-triplet conversion due to transmitter offset during SLIC was mitigated by turning off the temperature regulation within the NMR scanner, in order to minimize the change in temperature between the bore and the shuttling region above the magnet. The probe temperature within the bore was measured to be about 22 °C with the temperature regulation off, and the temperature during sample shuttling was not expected to vary more than ±5 °C from the probe temperature.

**Molecular dynamics simulations**

MD simulations in Amber20 were performed as described previously[28] with the following modifications: $PP_i$ was parametrized using ESP charges obtained from Gaussian 16 with B3LYP/6-31G(d), the polyphosphate parameters described by Meagher et al,[57] with the missing parameters provided by the GAFF2 force field. Minimization was performed in 5000 steps, Timesteps were 1 fs throughout, and the final isothermal/isobaric ensemble (NPT, 300 K, 1 bar) production run contained $10^7$ steps. The simulation was performed at 300 K. 100 snapshots were selected randomly to perform *ab initio* calculations of CSA tensors with the B3LYP/aug-cc-pVTZ combination and the GIAO method. Fig. S6 in the ESI shows the individual tensor norms and eigenvalues of the tensor components for all conformers. To calculate the average CSA tensors across all selected conformations, the molecules were aligned along the P-P vector (i.e. along the x coordinate) with the bridging P-O vector pointing upwards in the x-z plane, as shown in Fig. 4B. The CSA tensors were rotated into this frame and averaged. For the $R_1$ calculation, the Frobenius norms were taken of the symmetric and antisymmetric components of the average tensors. For the $R_S$ calculation, the Frobenius norm was calculated for the difference between the average tensors of each $^{31}P$. Tensor visualizations were generated using the Ovaloid function from SpinDynamica v3.6[58] in Mathematica, as described previously,[59, 60] and displayed with the MoleculePlot3D function.

The CSA tensor averaging procedure described above is strictly valid only in the limit where the internal motion is much faster than the overall tumbling rate. We justify its use as follows: from the MD trajectories the root mean square (rms) angular frequency of the $-PO_3^{2-}$ rotation around the bridging P-O bond is determined as 1.76 rad/ps. From this value, we can calculate the root-mean square rotation of $-PO_3^{2-}$ within the reorientation correlation time period determined above (48.6 ps) as 13.6π. We therefore can assume that the $-PO_3^{2-}$ rotation is much faster than the molecular reorientation, so that averaging the tensors for the two $^{31}P$ spins prior to taking the differences between them is the correct approach.

The second-rank correlation time was extracted from the MD runs for the reorientation of the P-P bond, which was 65.4 ps. The diffusion of the pyrophosphate molecule was calculated from the MD trajectory as $0.215 \cdot 10^{-9}$ $m^2/s$. The experimental diffusion coefficient determined by pulsed-field gradient NMR was $0.37 \cdot 10^{-9}$ $m^2/s$ (Fig. S7, ESI). Given the known relationships between rotational correlation times, diffusion coefficients, and viscosities, we therefore adjusted the correlation time obtained from computation by the factor 0.215/0.37, which resulted in a correlation time of 48.6 ps. This correlation time was further used in the spin dynamics simulations to obtain the relaxation rates.

## Author Contributions

Conceptualization: AJ
Formal analysis: DEK, AJ

Funding acquisition: MHL, AJ
Methodology: DEK, JL, MS, LB, AJ
Project administration: MHL, AJ
Resources: LB
Investigation: DEK, JL, MS, LD, LB
Visualization: DEK, AJ
Supervision: LB, MHL, AJ
Writing—original draft: DK, AJ
Writing—review & editing: DK, JL, LB, MHL, AJ

## Conflicts of interest

There are no conflicts to declare.

## Acknowledgements

D. E. K. thanks Christian Bengs and Jamie Whipham for helpful discussions regarding singlet NMR pulse sequences and NMR relaxation. The authors thank Alexey Kiryutin (International Tomography Centre, Novosibirsk, Russia) for sharing the shuttle design. This work was supported in part through the NYU IT High Performance Computing resources, services, and staff expertise (in particular by Dr Shenglong Wang).

Funding: National Science Foundation, award no. CHE 2108205 (AJ); Heising-Simons Foundation (AJ); Diamond Jubilee Visiting Fellowship, University of Southampton (AJ); EPSRC-UK, grant numbers EP/P009980/1, EP/T004320/1 and EP/P030491/1 (MHL); European Unions Horizon 2020 research and innovation programme, under the Marie Skłodowska-Curie grant agreement No 891400 (MHL); European Research Council, grant 786707-FunMagResBeacons (MHL).

## Notes and references

1. J. P. Yesinowski, R. J. Sunberg and J. J. Benedict, *Journal of Magnetic Resonance (1969)*, 1982, **47**, 85-90.
2. J. Kowalewski and L. Mäler, Taylor & Francis Group, LLC, Second edition. edn., 2018, p. 1 online resource.
3. J. W. Lee, *Journal of the Korean Chemical Society*, 1976, **20**, 364-373.
4. P. Håkansson, *Physical Chemistry Chemical Physics*, 2017, **19**, 10237-10254.
5. M. Odelius and J. Kowalewski, *J Chem Soc Faraday T*, 1995, **91**, 215-222.
6. J. Rantaharju and J. Vaara, *Phys Rev A*, 2016, **94**.
7. P. Hakansson, *Physical Chemistry Chemical Physics*, 2017, **19**, 10237-10254.
8. D. E. Korenchan, J. Lu, M. H. Levitt and A. Jerschow, *Phys Chem Chem Phys*, 2021, **23**, 19465-19471.
9. B. Kharkov, X. Duan, J. Rantaharju, M. Sabba, M. H. Levitt, J. W. Canary and A. Jerschow, *Phys Chem Chem Phys*, 2022, **24**, 7531-7538.
10. M. Carravetta, O. G. Johannessen and M. H. Levitt, *Phys Rev Lett*, 2004, **92**, 153003.
11. M. Carravetta and M. H. Levitt, *J Am Chem Soc*, 2004, **126**, 6228-6229.
12. G. Pileio, M. Concistre, M. Carravetta and M. H. Levitt, *J Magn Reson*, 2006, **182**, 353-357.
13. R. Sarkar, P. Ahuja, D. Moskau, P. R. Vasos and G. Bodenhausen, *Chemphyschem*, 2007, **8**, 2652-2656.
14. G. Pileio, M. Carravetta, E. Hughes and M. H. Levitt, *J Am Chem Soc*, 2008, **130**, 12582-12583.
15. G. Pileio, J. T. Hill-Cousins, S. Mitchell, I. Kuprov, L. J. Brown, R. C. Brown and M. H. Levitt, *J Am Chem Soc*, 2012, **134**, 17494-17497.
16. S. J. DeVience, R. L. Walsworth and M. S. Rosen, *J Magn Reson*, 2012, **218**, 5-10.
17. G. Stevanato, J. T. Hill-Cousins, P. Hakansson, S. S. Roy, L. J. Brown, R. C. Brown, G. Pileio and M. H. Levitt, *Angew Chem Int Ed Engl*, 2015, **54**, 3740-3743.
18. K. F. Sheberstov, H. M. Vieth, H. Zimmermann, B. A. Rodin, K. L. Ivanov, A. S. Kiryutin and A. V. Yurkovskaya, *Sci Rep*, 2019, **9**, 20161.
19. M. H. Levitt, in *Encyclopedia of Magnetic Resonance*2010.
20. M. H. Levitt, *Annu Rev Phys Chem*, 2012, **63**, 89-105.
21. M. H. Levitt, G. Stevanato, G. Pileio, L. J. Brown, C. Bengs, R. Pigliapochi, A. Jerschow, S. J. DeVience, M. S. Rosen, A. S. Kiryutin, B. A. Rodin, N. N. Lukzen, A. V. Yurkovskaya, H. M. Vieth, K. L. Ivanov, M. C. D. Tayler, B. Roberto, A. Sadet, V. Nastasa, P. Ghenuche, P. R. Vasos, R. Sarkar, M. Tourell, A. M. Torres, W. S. Price, T. S. Mahesh, D. Khurana, K. Munnemann, L. Buljubasich, M. B. Franzoni, S. S. Roy, F. Teleanu, G. Bodenhausen, J. N. Dumez, S. J. Elliott, I. V. Zhukov and D. Budker, *Long-lived Nuclear Spin Order: Theory and Applications*, Royal Society of Chemistry2020.
22. F. Teleanu, A. Sadet and P. R. Vasos, *Prog Nucl Magn Reson Spectrosc*, 2021, **122**, 63-75.
23. G. Pileio, M. Carravetta and M. H. Levitt, *Proc Natl Acad Sci U S A*, 2010, **107**, 17135-17139.
24. G. Pileio, S. Bowen, C. Laustsen, M. C. Tayler, J. T. Hill-Cousins, L. J. Brown, R. C. Brown, J. H. Ardenkjaer-Larsen and M. H. Levitt, *J Am Chem Soc*, 2013, **135**, 5084-5088.
25. G. Pileio, J. N. Dumez, I. A. Pop, J. T. Hill-Cousins and R. C. Brown, *J Magn Reson*, 2015, **252**, 130-134.
26. R. Sarkar, P. R. Vasos and G. Bodenhausen, *J Am Chem Soc*, 2007, **129**, 328-334.
27. S. Cavadini, J. Dittmer, S. Antonijevic and G. Bodenhausen, *J Am Chem Soc*, 2005, **127**, 15744-15748.
28. S. J. Elliott, L. J. Brown, J. N. Dumez and M. H. Levitt, *J Magn Reson*, 2016, **272**, 87-90.
29. B. Kharkov, X. Duan, E. S. Tovar, J. W. Canary and A. Jerschow, *Phys Chem Chem Phys*, 2019, **21**, 2595-2600.
30. C. Bengs, M. Sabba, A. Jerschow and M. H. Levitt, *Phys Chem Chem Phys*, 2020, **22**, 9703-9712.
31. B. Kharkov, X. Duan, J. W. Canary and A. Jerschow, *J Magn Reson*, 2017, **284**, 1-7.
32. S. J. DeVience, R. L. Walsworth and M. S. Rosen, *Phys Rev Lett*, 2013, **111**, 173002.
33. A. S. Kiryutin, A. N. Pravdivtsev, A. V. Yurkovskaya, H. M. Vieth and K. L. Ivanov, *J Phys Chem B*, 2016, **120**, 11978-11986.
34. A. N. Pravdivtsev, A. S. Kiryutin, A. V. Yurkovskaya, H. M. Vieth and K. L. Ivanov, *J Magn Reson*, 2016, **273**, 56-64.
35. B. A. Rodin, A. S. Kiryutin, A. V. Yurkovskaya, K. L. Ivanov, S. Yamamoto, K. Sato and T. Takui, *J Magn Reson*, 2018, **291**, 14-22.
36. G. Pileio, *Prog Nucl Magn Reson Spectrosc*, 2017, **98-99**, 1-19.
37. S. Mamone, N. Rezaei-Ghaleh, F. Opazo, C. Griesinger and S. Gloggler, *Sci Adv*, 2020, **6**, eaaz1955.

38. S. J. Devience, R. L. Walsworth and M. S. Rosen, *NMR Biomed*, 2013, **26**, 1204-1212.
39. S. J. DeVience, R. L. Walsworth and M. S. Rosen, *Journal of Magnetic Resonance*, 2021, **333**.
40. M. P. A. Fisher, *Annals of Physics*, 2015, **362**, 593-602.
41. M. C. Tayler and M. H. Levitt, *J Am Chem Soc*, 2013, **135**, 2120-2123.
42. C. Bengs, L. Dagys, G. A. I. Moustafa, J. W. Whipham, M. Sabba, A. S. Kiryutin, K. L. Ivanov and M. H. Levitt, *J Chem Phys*, 2021, **155**, 124311.
43. H. J. Hogben, M. Krzystyniak, G. T. Charnock, P. J. Hore and I. Kuprov, *J Magn Reson*, 2011, **208**, 179-194.
44. D. A. Case, I. Y. Ben-Shalom, S. R. Brozell, D. S. Cerutti, T. E. Cheatham III, V. W. D. Cruzeiro, T. A. Darden, R. E. Duke, D. Ghoreishi, G. Giambasu, T. Giese, M. K. Gilson, H. Gohlke, A. W. Goetz, D. Greene, R. Harris, N. Homeyer, Y. Huang, S. Izadi, A. Kovalenko, R. Krasny, T. Kurtzman, T. S. Lee, S. LeGrand, P. Li, C. Lin, J. Liu, T. Luchko, R. Luo, V. Man, D. J. Mermelstein, K. M. Merz, Y. Miao, G. Monard, C. Nguyen, H. Nguyen, A. Onufriev, F. Pan, R. Qi, D. R. Roe, A. Roitberg, C. Sagui, S. Schott-Verdugo, J. Shen, C. L. Simmerling, J. Smith, J. Swails, R. C. Walker, J. Wang, H. Wei, L. Wilson, R. M. Wolf, X. Wu, L. Xiao, Y. Xiong, D. M. York and P. A. Kollman, in *AMBER 2020*, University of California, San Francisco2020.
45. G. Pileio, J. T. Hill-Cousins, S. Mitchell, I. Kuprov, L. J. Brown, R. C. Brown and M. H. Levitt, *Journal of the American Chemical Society*, 2012, **134**, 17494-17497.
46. D. E. Korenchan, J. Lu, M. H. Levitt and A. Jerschow, *Physical Chemistry Chemical Physics*, 2021, **23**, 19465-19471.
47. G. Pileio, *Progress in nuclear magnetic resonance spectroscopy*, 2010, **56**, 217-231.
48. R. E. D. McClung, in *Encyclopedia of Magnetic Resonance*2007.
49. H. W. Spiess, in *Dynamic NMR spectroscopy*, Springer-Verlag, Berlin ; New York1978, p. 214 p.
50. M. C. Tayler and M. H. Levitt, *Phys Chem Chem Phys*, 2011, **13**, 9128-9130.
51. C. P. Weingarten, P. M. Doraiswamy and M. P. Fisher, *Front Hum Neurosci*, 2016, **10**, 541.
52. T. Yan, H. Zhang, Y. Liu, W. Guan, J. Long, W. Li and J. You, *RSC Adv.*, 2014, **4**, 37220-37230.
53. L. Zervas and I. Dilaris, *J. Am. Chem. Soc.*, 1955, **77**, 5354-5357.
54. F. Gao, X. Yan, T. Shakya, O. M. Baettig, S. Ait-Mohand-Brunet, A. M. Berghuis, G. D. Wright and K. Auclair, *J. Med. Chem.*, 2006, **49**, 5273-5281.
55. J. R. Falck, K. K. Reddy, J. Ye, M. Saady, C. Mioskowski, S. B. Shears, Z. Tan and S. Safrany, *J. Am. Chem. Soc.*, 1995, **117**, 12172-12175.
56. I. V. Zhukov, A. S. Kiryutin, A. V. Yurkovskaya, Y. A. Grishin, H.-M. Vieth and K. L. Ivanov, *Physical Chemistry Chemical Physics*, 2018, **20**, 12396-12405.
57. K. L. Meagher, L. T. Redman and H. A. Carlson, *Journal of Computational Chemistry*, 2003, **24**, 1016-1025.
58. C. Bengs and M. H. Levitt, *Magn Reson Chem*, 2018, **56**, 374-414.
59. R. Radeglia, *Solid State Nucl Magn Reson*, 1995, **4**, 317-321.
60. R. P. Young, C. R. Lewis, C. Yang, L. Wang, J. K. Harper and L. J. Mueller, *Magn Reson Chem*, 2019, **57**, 211-223.